THE VERTICAL COMPOSITION OF NEUTRINO-DOMINATED ACCRETION DISKS IN GAMMA-RAY BURSTS

Tong Liu[1], Li Xue[1,2], Wei-Min Gu[1,3], and Ju-Fu Lu[1]

[1] Department of Physics and Institute of Theoretical Physics and Astrophysics, Xiamen University, Xiamen, Fujian 361005, China; tongliu@xmu.edu.cn
[2] Nicolaus Copernicus Astronomical Center, Bartycka 18, 00-716 Warszawa, Poland
[3] Harvard-Smithsonian Center for Astrophysics, 60 Garden Street, Cambridge, MA 02138, USA

ABSTRACT

We investigate the vertical structure and element distribution of neutrino-dominated accretion flows around black holes in spherical coordinates using the reasonable nuclear statistical equilibrium. According to our calculations, heavy nuclei tend to be produced in a thin region near the disk surface, whose mass fractions are primarily determined by the accretion rate and vertical distribution of temperature and density. In this thin region, we find that ^{56}Ni is dominant for the flow with a low accretion rate (e.g., 0.05 $M_\odot$ s^{-1}), but ^{56}Fe is dominant for the flow with a high accretion rate (e.g., 1 $M_\odot$ s^{-1}). The dominant ^{56}Ni in the aforementioned region may provide a clue to understanding the bumps in the optical light curve of core-collapse supernovae.

Key words: accretion, accretion disks – black hole physics – gamma-ray burst: general – nuclear reactions, nucleosynthesis, abundances

Online-only material: color figure

1. INTRODUCTION

The popular model of the central engine in gamma-ray bursts (GRBs), called neutrino-dominated accretion flows (NDAFs, see, e.g., Popham et al. 1999; Narayan et al. 2001; Kohri & Mineshige 2002; Di Matteo et al. 2002; Kohri et al. 2005; Lee et al. 2005; Gu et al. 2006; Chen & Beloborodov 2007; Liu et al. 2007, 2008, 2010a, 2010b, 2012; Kawanaka & Mineshige 2007; Sun et al. 2012), involves a hyperaccreting spinning stellar black hole with mass accretion rates in the range of 0.01–10 $M_\odot$ s^{-1}. In general, low (such as 0.05 $M_\odot$ s^{-1}) and high (1 $M_\odot$ s^{-1}) mass accretion rates correspond to long ($T_{90} > 2$ s) and short ($T_{90} < 2$ s) duration GRBs, respectively, which originate from collapsar (Woosley 1993; Paczyński 1998) and the merger of two neutron stars or a neutron star and a black hole (Eichler et al. 1989; Paczyński 1991; Narayan et al. 1992), respectively. The model can give reasonable explanations of the progenitor and energetics of fireballs in GRBs by the neutrino annihilation or magnetohydrodynamic processes. The extreme state is a hotbed to produce heavy elements, and the central region of GRBs is an ideal location to supply an extremely hot and dense state. Actually, nucleosynthesis should also be involved in the NDAF model. Liu et al. (2007) studied the radial structure and neutrino annihilation luminosity of NDAFs. We assumed that the heaviest nucleus is ^{4}He, which implies that the numerical value of the electron fraction at the radial outer boundary is 0.5. Liu et al. (2008) studied the vertical structure and luminosity of NDAFs under the above assumption. Kawanaka & Mineshige (2007) assumed that the inflowing gas is composed primarily of neutron-rich iron group nuclei, and that the electron fraction is 0.42, then they studied the radial structure and stability of NDAFs for the different mass accretion rate, using a realistic equation of state (Lattimer & Swesty 1991) in order to properly treat the dissociation of nuclei. Unfortunately, they did not provide more information on heavy nuclei. To our knowledge, the self-consistent vertical distribution of elements without making a limit for the electron fraction has not been previously investigated.

The purpose of this paper is to investigate the element distribution in the vertical direction of NDAFs using detailed neutrino physics and precise nuclear statistical equilibrium (NSE). The plan is as follows. In Section 2, with the self-similar assumption in the radial direction, we numerically solve the differential equations of NDAFs in the vertical direction with the proton-rich NSE (Seitenzahl et al. 2008) and reasonable boundary condition. In Section 3, we present the vertical distribution of physical quantities, such as the density, temperature, and electron fraction, and show the mass fractions of the main elements at various radii for the different mass accretion rates. We discuss our findings and present conclusions in Section 4.

2. EQUATIONS AND BOUNDARY CONDITION

2.1. Equations

In order to facilitate a self-similar process, we adopt the Newtonian potential $\psi = -GM/r$, where M is the mass of the central black hole, and suppose the accretion flow is time-independent and axisymmetric in spherical coordinates (r, θ, ϕ), i.e., $\partial/\partial t = \partial/\partial \phi = 0$.

The basic equations are composed of continuity and momentum equations (see, e.g., Narayan & Yi 1995; Xue & Wang 2005). The self-similar assumptions are adopted in the radial direction to simplify the hydrodynamic equations, and the vertical velocity is ignored ($v_\theta = 0$). We then obtain the vertical hydrodynamic equations as follows (Gu et al. 2009; Liu et al. 2010a, 2012):

$$\frac{1}{2}v_r{}^2 + \frac{5}{2}c_s{}^2 + v_\phi{}^2 - r^2\Omega_K{}^2 = 0, \tag{1}$$

$$\frac{1}{\rho}\frac{dp}{d\theta} = v_\phi{}^2 \cot\theta, \tag{2}$$

$$v_r = -\frac{3}{2}\frac{\alpha c_s{}^2}{r\Omega_K}, \tag{3}$$

where v_r and v_ϕ are the radial and azimuthal components of the velocity, the sound speed c_s is defined as $c_s^2 = p/\rho$, the

Keplerian angular velocity is $\Omega_K = (GM/r^3)^{1/2}$, and α is a constant viscosity parameter.

Furthermore, according the continuity equation, the mass accretion rate can be written as

$$\dot{M} = -4\pi r^2 \int_{\theta_0}^{\pi/2} \rho v_r \sin\theta d\theta, \tag{4}$$

where ρ is the density, and θ_0 and $\pi/2$ are the polar angle of the surface and equatorial plane, respectively.

The total pressure is expressed as the sum of four pressures:

$$p = p_{gas} + p_{rad} + p_e + p_\nu, \tag{5}$$

where p_{gas}, p_{rad}, p_e, and p_ν are the gas pressure from nucleons, the radiation pressure of photons, the degeneracy pressure of electrons, and the radiation pressure of neutrinos, respectively. Detailed expressions of the pressure components were given in Liu et al. (2007). Additionally, we assume the polytropic relation in the vertical direction, $p = K\rho^{4/3}$, where K is a constant and $\gamma = 4/3$ is the adiabatic index.

Considering the energetic balance, the energy equation is written as (Liu et al. 2010a, 2012)

$$Q_{vis} = Q_{adv} + Q_\nu, \tag{6}$$

where Q_{vis}, Q_{adv}, and Q_ν are the viscous heating, advective cooling, and neutrino cooling rates per unit area, respectively. We ignore the cooling of the photodisintegration of α-particles and other heavier nuclei (Liu et al. 2010a, 2012). The viscous heating rate per unit volume $q_{vis} = \nu\rho r^2 [\partial(v_\phi/r)/\partial r]^2$ and the advective cooling rate per unit volume $q_{adv} = \rho v_r(\partial e/\partial r - (p/\rho^2)\partial\rho/\partial r)$ (e is the internal energy per unit volume) are expressed, after self-similar simplification, as

$$q_{vis} = \frac{9}{4}\frac{\alpha p v_\phi^2}{r^2 \Omega_K}, \tag{7}$$

$$q_{adv} = -\frac{3}{2}\frac{(p - p_e)v_r}{r}, \tag{8}$$

where the entropy of degenerate particles is neglected. Thus the vertical integration of Q_{vis} and Q_{adv} are the following (Liu et al. 2010a, 2012):

$$Q_{vis} = 2\int_{\theta_0}^{\frac{\pi}{2}} q_{vis} r \sin\theta d\theta, \tag{9}$$

$$Q_{adv} = 2\int_{\theta_0}^{\frac{\pi}{2}} q_{adv} r \sin\theta d\theta. \tag{10}$$

The cooling due to the neutrino radiation Q_ν can be defined as (Lee et al. 2005; Liu et al. 2012)

$$Q_\nu = 2\sum_k \int_{\theta_0}^{\frac{\pi}{2}} q_{\nu_k} e^{-\tau_{\nu_k}} r \sin\theta d\theta , \tag{11}$$

where k represents different types of neutrinos and antineutrinos, and q_{ν_k} is the sum of the cooling rates per unit volume due to the Urca processes, electron–positron pair annihilation, nucleon–nucleon bremsstrahlung, and Plasmon decay, hereafter represented as q_i ($i = 1, 2, 3, 4$), respectively. The optical depth

of the neutrino τ_{ν_k}, which includes absorption τ_{a,ν_k} and scattering τ_{s,ν_k}, is written as

$$\tau_{\nu_k} = \tau_{a,\nu_k} + \tau_{s,\nu_k}, \tag{12}$$

where the two optical depths can be defined as

$$\tau_{a,\nu_k} \approx \sum_i \frac{\int_{\theta_0}^\theta 2q_i r d\theta}{7\sigma T^4}, \tag{13}$$

$$\tau_{s,\nu_k} \approx \sum_j \int_{\theta_0}^\theta \sigma_j n_j r d\theta, \tag{14}$$

where σ_j and n_j ($j = 1, 2, 3, 4$) are the cross sections and the number density of protons, neutrons, α-particles, and electrons, respectively (e.g., Kohri et al. 2005; Chen & Beloborodov 2007). It is noteworthy that different types of neutrinos involve different processes (for details, see Liu et al. 2007), though for simplicity we still show the sum of all the cooling rates for any type of neutrinos or antineutrinos as Equation (13). We ignore the absorption and scattering reaction by the heavy nuclei in the model. In order to embody the complicated microphysics in NDAFs, we assume that the disk is optically thin to neutrinos with a mass accretion rate less than $2 M_\odot \, \mathrm{s}^{-1}$, which was indicated by Liu et al. (2007, 2012). The electron fraction can be defined as

$$Y_e = \frac{n_p}{n_n + n_p}, \tag{15}$$

where n_p and n_n are the total number density of protons and neutrons, respectively, which have to satisfy the condition of electrical neutrality and the chemical potential equilibrium (e.g., Liu et al. 2007).

Liu et al. (2007) calculated the electron fraction according to the simple NSE equation, the condition of electrical neutrality, and a bridging formula of electron fraction that is valid in both the optically thin and thick regimes. In this paper, we use the strict NSE equations (see Section 2.2) to replace the simple one, which assumed that the heaviest nuclei is ^{4}He. Meanwhile, the condition of electrical neutrality still holds and can be written as

$$\frac{\rho Y_e}{m_u} = n_{e^-} - n_{e^+}, \tag{16}$$

where m_u is the mean mass of nucleus, and n_{e^-} and n_{e^+} are the number density of electron and positron, respectively, which can be given by the Fermi–Dirac distribution (Liu et al. 2007).

Furthermore, if Z_i and N_i are defined as the number of the protons and neutrons of a nucleus X_i, and its number density (approximately equals the mass fraction) is n_i, then the electron fraction can also be written as

$$Y_e = \sum_i n_i Z_i \bigg/ \sum_i n_i(Z_i + N_i). \tag{17}$$

However, we assume that the disk is optically thin to neutrinos, the previous bridging formula of the electron fraction can be simplified as (e.g., Yuan 2005; Liu et al. 2007)

$$\lg\frac{\tilde{n}_n}{\tilde{n}_p} = \frac{2\mu_e - Q}{k_B T}, \tag{18}$$

where μ_e and Q are the chemical potential and rest-mass energy difference between neutron and proton, respectively. $\tilde{n}_n$ and $\tilde{n}_p$ are the number density of the free neutrons and protons, respectively, corresponding to the nucleus with $Z = 0$, $N = 1$ and $Z = 1$, $N = 0$ in Equation (17).

2.2. Nucleosynthesis

In our calculations, the NSE equations are required to be applicable for all the variations of the electron fraction. NSE established by all nuclear reactions are in the chemical equilibrium. The complicated and detailed balance has been included under the condition of the equilibrium of chemical potential. Seitenzahl et al. (2008) studied proton-rich material in a state of NSE, which applies to almost the whole range of the electron fraction. They showed that ^{56}Ni is favored in NSE under proton-rich conditions ($Y_e \simeq 0.5$), being different from the case of domination by the Fe-peak nuclei with the largest binding energy per nucleon, that have a proton-to-nucleon ratio close to the prescribed electron fraction. Particularly, the lower limit of the temperature in the NSE calculation is identified as about 2×10^9 K (Seitenzahl et al. 2008). If the temperature is lower than this limit, the NSE solutions will not be reliable. Therefore, in our calculations we assume that all nuclear reactions would cease when the temperature is lower than this limit because this limit is near the surface temperature and the components change little under it (Seitenzahl et al. 2008). The NSE code in proton-rich environments can be downloaded from http://cococubed.asu.edu/code_pages/nse.shtml. In the NSE, the independent variables are the density ρ, temperature T, and electron fraction Y_e, which are essential in the vertical NDAF model according to the description above.

2.3. Boundary Condition

Naturally, if the gradient of radiation pressure is larger than the gravity, outflows may occur, so we decided that the gradient could present a boundary condition for the accretion disk. Here we deviated from Liu et al. (2010a) and set boundary conditions to be the mechanical equilibrium, like solving the principle of Eddington luminosity. Furthermore, we can ignore the radial gradient of radial velocity and pressure at the surface of the disk. There are three forces to balance, namely gravity, radiation force, and centrifugal force in non-inertial reference frame. It should be pointed out that NDAFs are extremely optically thick for photons, so the radiation pressure of photons anywhere can be written as

$$p_{\rm rad} = \frac{1}{3}aT^4, \qquad (19)$$

where a is the radiation constant and T is the temperature of gas. The mechanical equilibrium can be written as (Liu et al. 2012)

$$p_{\rm rad}\,|_{\theta=\theta_0}\,\sigma_{\rm T} = \frac{2GMm_u}{r^2}\cot\theta_0. \qquad (20)$$

Combined with Equation (19), the surface temperature can be derived as (Liu et al. 2012)

$$T\,|_{\theta=\theta_0} = \left(\frac{6GMm_u}{a\sigma_{\rm T}r^2}\cot\theta_0\right)^{\frac{1}{4}}, \qquad (21)$$

where m_u is the mean mass of a nucleon and $\sigma_{\rm T}$ is the Thompson scattering cross. Since the NSE and boundary condition are taken into account, the complete equations of our model are established.

3. NUMERICAL RESULTS

Figure 1 shows the variations of the density ρ, temperature T, and electron fraction Y_e with θ. The solid and dashed lines
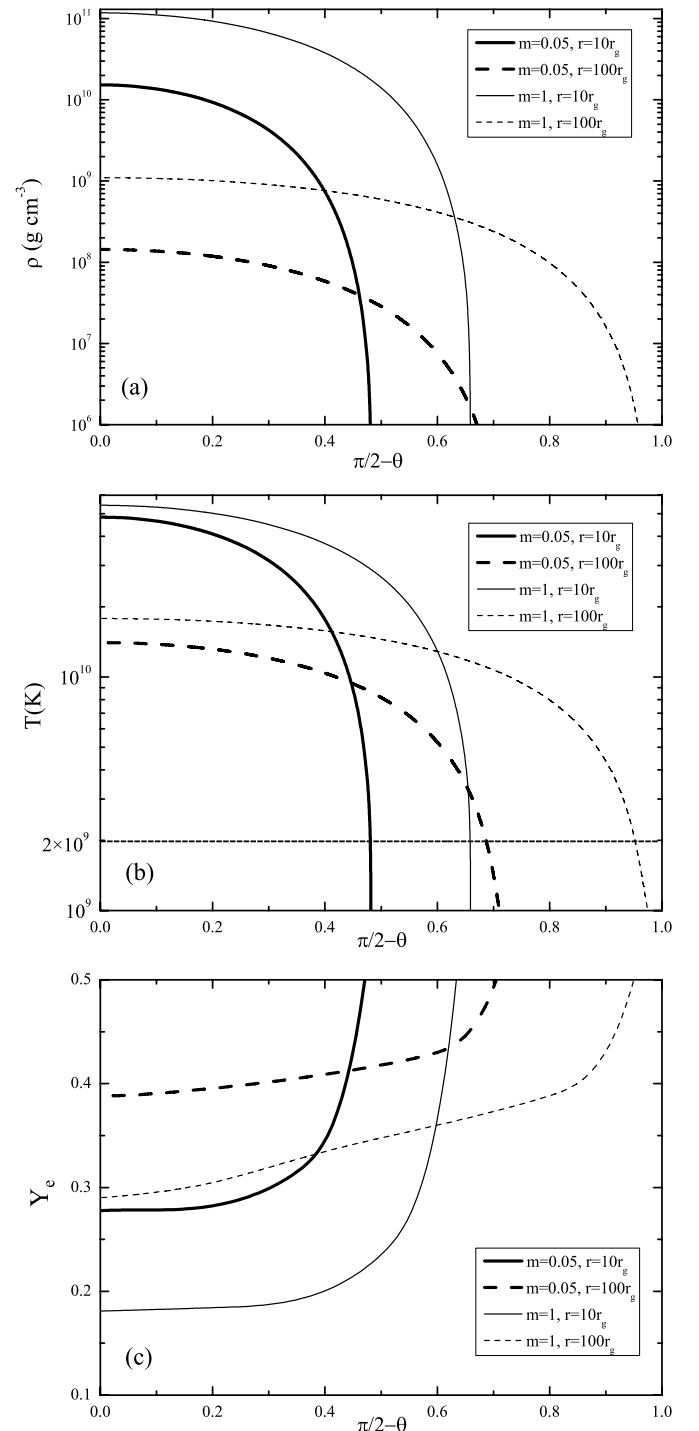
Figure 1. Variations of the density ρ, temperature T, and electron fraction Y_e with θ at $r = 10r_g$ (solid lines) and $100r_g$ (dashed lines) for $\dot{M} = m\, M_\odot$ s^{-1}, where $m = 0.05$ (thick lines) and 1 (thin lines).

represent the solutions at $r = 10r_g$ and $100r_g$, respectively, whereas $r_g = 2GM/c^2$ is the Schwarzschild radius, and the thick and thin lines indicate the solutions for $\dot{M} = 0.05\, M_\odot$ s^{-1} and $1\, M_\odot$ s^{-1}, respectively. The variations of the density, temperature, and electron fraction are similar to the solutions in Liu et al. (2010a, 2012). We marked the lower limit of the temperature $\sim 2 \times 10^9$ K in NSE equations in Figure 1(b). $\dot{M} = 0.05\, M_\odot$ s^{-1} and $\dot{M} = 1\, M_\odot$ s^{-1} correspond to Y_e around 0.49 and 0.47 near the disk surface, respectively. The half-opening angles of the
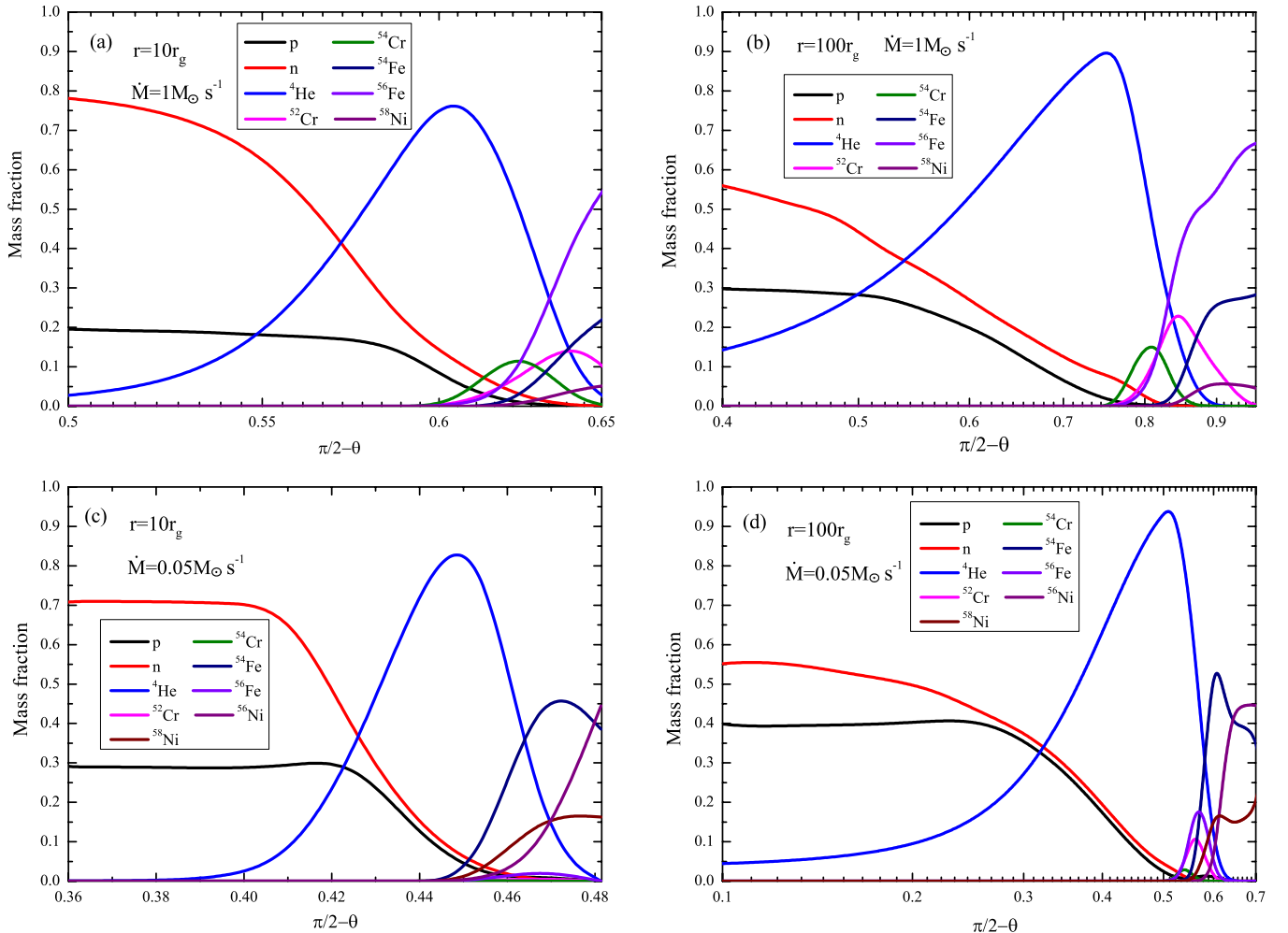
Figure 2. Variations of the mass fraction of the main elements with θ at $r = 10r_g$ and $100r_g$ for $\dot{M} = 0.05\ M_\odot\ \mathrm{s}^{-1}$ and $1\ M_\odot\ \mathrm{s}^{-1}$.
(A color version of this figure is available in the online journal.)

disks are also similar to those in Liu et al. (2012), which have the positive correlation with the accretion rate and radius.

Figure 2 shows the variations of the mass fraction (approximately equals to the number density) of the free neutron and proton and main elements (including ^{4}He, ^{52}Cr, ^{54}Cr, ^{54}Fe, ^{56}Fe, ^{56}Ni, and ^{58}Ni, corresponding to the lines with different colors) with θ at $r = 10r_g$ and $100r_g$ for $\dot{M} = 0.05\ M_\odot\ \mathrm{s}^{-1}$ and $1\ M_\odot\ \mathrm{s}^{-1}$ corresponding to panels (a)–(d). In addition, according to Equation (17), the profiles of Y_e can be indicated by Figure 2. Furthermore, the open angles in different cases correspond to the lower limit of the temperature in NSE code in Figure 1(b), which is the limit of open angle in Figure 2. We consider that the nuclear reaction will not occur under this temperature limit. ^{56}Ni dominates at the disk surface for $\dot{M} = 0.05\ M_\odot\ \mathrm{s}^{-1}$, and ^{56}Fe dominates for $\dot{M} = 1\ M_\odot\ \mathrm{s}^{-1}$, corresponding to Y_e around 0.49 and 0.47, respectively. Other heavy nuclei also appear in these cases. The solutions show that the proportion of the nuclear matter increases with the radius at the same accretion rate. The mass fraction of ^{56}Ni or ^{56}Fe near the surface also increases with radius. In the middle region, ^{4}He is dominant for all accretion rates. The free neutrons and protons are dominant near the equatorial plane of the disk in the hot and dense state; most of the free protons turn into the free neutrons due to the Urca process (see, e.g., Liu et al. 2007), which causes the dominant free neutrons and the decrease of electron fraction. In the model,

the accretion rate determines the density and temperature. Furthermore, the radial and vertical distribution of the density and temperature determines the electron fraction and element distribution. In simple terms, the change of the electron fraction is inversely associated with the accretion rate and radius when the free baryons dominate.

4. DISCUSSION AND CONCLUSIONS

4.1. Discussion

Supernova light curve bumps have been observed in the optical afterglow of some long-duration GRBs, which are driven by the decay of ^{56}Ni (e.g., Galama et al. 1999; Woosley & Bloom 2006). How to produce massive ^{56}Ni in supernovae accompanied by GRBs is a major problem that remains unsolved. It is possible that ^{56}Ni originates from the central engine transported by the outflow (e.g., MacFadyen & Woosley 1999; MacFadyen 2003; Surman et al. 2011) or the explosive burning (e.g., Maeda & Nomoto 2003; Maeda & Tominaga 2009). Moreover, the detection of Fe Kα X-ray lines can play an important role in understanding the nature of GRBs (e.g., Lazzati et al. 1999; Kallman et al. 2003; Gou et al. 2005; Butler 2007). Observations of some X-ray afterglows by *BeppoSAX*, *ASCA*, and *Chandra* have revealed strong Fe Kα emission lines (e.g., Piro et al. 2000). Reeves et al. (2002) reported on an

XMM-Newton observation of the X-ray afterglow of long-duration GRB 011211. The X-ray spectrum reveals evidence of emission lines of magnesium, silicon, sulfur, argon, calcium, and possibly nickel, arising in enriched material with an outflow velocity on the order of $0.1c$. Nevertheless, there are no further observations on the metal lines in GRBs since the launch of *Swift*. There is scarcely any observational evidence on Fe Kα lines appearing in the X-ray afterglow of short-duration GRBs. Recently, many works have focused on how the heavy nuclei are produced by the central engine of GRBs. Surman et al. (2011) studied the nucleosynthesis, particularly for the progenitor of ^{56}Ni in the hot outflows from GRB accretion disks. Metzger et al. (2011) suggested that the composition of ultrahigh energy cosmic rays becomes dominated by heavy nuclei at high energies forming GRB jets or outflows (also see Sigl et al. 1995; Horiuchi et al. 2012). Metzger (2012) investigated the steady-state models of accretion disks produced by the tidal disruption of a white dwarf by a neutron star or stellar black hole, which can produce heavier elements via burning the initial material of the white dwarf. They discussed the recently discovered subluminous Type I supernovae that result from those mergers.

When a massive star collapses to a black hole, a powerful supernova occurs. The newborn hyperaccreting black hole may power a GRB. The optical light curve bumps of the supernovae accompanied with GRBs are driven by the decay of ^{56}Ni in the outflows coming from the central engine. We have described self-consistently how to produce ^{56}Ni and other elements in the central region of GRBs with the NDAF model. Only at the low accretion rate exactly corresponding to long GRBs does ^{56}Ni dominate near the disk surface. More daringly, if the outflow occurs from the disk surface, which consists of ^{56}Ni and other heavy nuclei, the bumps in supernova light curve can be naturally generated due to ^{56}Ni decay in the outflow from NDAFs. Liu et al. (2012) revisited the vertical structure of NDAFs and showed that the possible outflow may appear in the outer region of the disk according to the calculations of the vertical distribution of the Bernoulli parameter. Furthermore, we noticed that the gradient of radiation pressure may be larger than the gravity in the region out of the boundary, which has been represented in Section 2.3. Part of the material near the surface will become outflow pushed out by the radiation pressure. We also noticed that the description of NDAF is similar to that of the slim disk. The high-speed outflow may be generated near the disk surface in the two-dimensional simulations of a supercritical disk (e.g., Ohsuga et al. 2005; Ohsuga 2007; Ohsuga & Mineshige 2011). All these suggest that the outflow near the disk surface may appear in the NDAF model.

The nickel in the outflows from the surface of NDAF with a low-mass accretion rate may be the most important source of the long-duration GRB ^{56}Ni production. Analogously, iron and other heavy nuclei may also form the outflow injecting into the external environment in GRBs. A NDAF model with outflows needs to be constructed for further theoretical explanation of the bumps in the optical light curve of core-collapse supernovae.

4.2. Conclusions

In this paper, we revisit the vertical element distribution of NDAFs around black holes in spherical coordinates with detailed neutrino physics and precise NSE and discuss the vertical element distribution in the solutions. The major points are as follows:

1. The heavy elements distribute near the surface of the disk and the free protons and neutrons dominate near the equatorial plane. The distribution of the density and temperature determines the nuclear matter distribution.
2. In the region near the surface of NDAFs, nickel will be dominant for low-mass accretion rates, whereas iron will be dominant for high accretion rates. The dominant ^{56}Ni may provide a clue to understanding the bumps in the optical light curve of core-collapse supernovae.

REFERENCES

Butler, N. R. 2007, ApJ, 656, 1001
Chen, W.-X., & Beloborodov, A. M. 2007, ApJ, 657, 383
Di Matteo, T., Perna, R., & Narayan, R. 2002, ApJ, 579, 706
Eichler, D., Livio, M., Piran, T., & Schramm, D. N. 1989, Natur, 340, 126
Galama, T. J., Briggs, M. S., Wijers, R. A. M. J., et al. 1999, Natur, 398, 394
Gou, L. J., Mészáros, P., & Kallman, T. R. 2005, ApJ, 624, 889
Gu, W.-M., Liu, T., & Lu, J.-F. 2006, ApJL, 643, 87
Gu, W.-M., Xue, L., Liu, T., & Lu, J.-F. 2009, PASJ, 61, 1313
Horiuchi, S., Murase, K., Ioka, K., & Meszaros, P. 2012, ApJ, 753, 69
Kallman, T. R., Mészáros, P., & Rees, M. J. 2003, ApJ, 593, 946
Kawanaka, N., & Mineshige, S. 2007, ApJ, 662, 1156
Kohri, K., & Mineshige, S. 2002, ApJ, 577, 311
Kohri, K., Narayan, R., & Piran, T. 2005, ApJ, 629, 341
Lattimer, J. M., & Swesty, D. F. 1991, NuPhA, 535, 331
Lazzati, D., Campana, S., & Ghisellini, G. 1999, MNRAS, 304, L31
Lee, W. H., Ramirez-Ruiz, E., & Page, D. 2005, ApJ, 632, 421
Liu, T., Gu, W.-M., Dai, Z.-G., & Lu, J.-F. 2010a, ApJ, 709, 851
Liu, T., Gu, W.-M., Xue, L., & Lu, J.-F. 2007, ApJ, 661, 1025
Liu, T., Gu, W.-M., Xue, L., & Lu, J.-F. 2012, Ap&SS, 337, 711
Liu, T., Gu, W.-M., Xue, L., Weng, S.-S., & Lu, J.-F. 2008, ApJ, 676, 545
Liu, T., Liang, E.-W., Gu, W.-M., et al. 2010b, A&A, 516, A16
MacFadyen, A. I. 2003, BAAS, 35, 1363
MacFadyen, A. I., & Woosley, S. E. 1999, ApJ, 524, 262
Maeda, K., & Nomoto, K. 2003, ApJ, 598, 1163
Maeda, K., & Tominaga, N. 2009, MNRAS, 394, 1317
Metzger, B. D. 2012, MNRAS, 419, 827
Metzger, B. D., Giannios, D., & Horiuchi, S. 2011, MNRAS, 415, 2495
Narayan, R., Paczynski, B., & Piran, T. 1992, ApJL, 395, 83
Narayan, R., Piran, T., & Kumar, P. 2001, ApJ, 557, 949
Narayan, R., & Yi, I. 1995, ApJ, 444, 231
Ohsuga, K. 2007, ApJ, 659, 205
Ohsuga, K., & Mineshige, S. 2011, ApJ, 736, 2
Ohsuga, K., Mori, M., Nakamoto, T., & Mineshige, S. 2005, ApJ, 628, 368
Paczyński, B. 1991, AcA, 41, 257
Paczyński, B. 1998, ApJL, 494, 45
Piro, L., Garmire, G., Garcia, M., et al. 2000, Sci, 290, 955
Popham, R., Woosley, S. E., & Fryer, C. 1999, ApJ, 518, 356
Reeves, J. N., Watson, D., Osborne, J. P., et al. 2002, Natur, 416, 512
Seitenzahl, I. R., Timmes, F. X., Marin-Laflèche, A., et al. 2008, ApJL, 685, 129
Sigl, G., Jedamzik, K., Schramm, D. N., & Berezinsky, V. S. 1995, PhRvD, 52, 6682
Sun, M.-Y., Liu, T., Gu, W.-M., & Lu, J.-F. 2012, ApJ, 752, 31
Surman, R., McLaughlin, G. C., & Sabbatino, N. 2011, ApJ, 743, 155
Woosley, S. E. 1993, ApJ, 405, 273
Woosley, S. E., & Bloom, J. S. 2006, ARA&A, 44, 507
Xue, L., & Wang, J. 2005, ApJ, 623, 372
Yuan, Y.-F. 2005, PhRvD, 72, 013007